

## DNA Condensation

## Lipophilic Tetranuclear Ruthenium(II) Complexes as Two-Photon Luminescent Tracking Non-Viral Gene Vectors

Bole Yu,<sup>[a, b]</sup> Cheng Ouyang,<sup>[a]</sup> Kangqiang Qiu,<sup>[a]</sup> Jing Zhao,<sup>[b]</sup> Liangnian Ji,<sup>[a]</sup> and Hui Chao\*<sup>[a]</sup>

**Abstract:** Fluorescence detection is the most effective tool for tracking gene delivery in living cells. To reduce photodamage and autofluorescence and to increase deep penetration into cells, choosing appropriate fluorophores that are capable of two-photon activation under irradiation in the NIR or IR regions is an effective approach. In this work, we have developed six tetranuclear ruthenium(II) complexes, **GV1–6**, and have studied their one- and two-photon luminescence properties. DNA interaction studies have demonstrated that **GV2–6**, bearing hydrophobic alkyl ether chains, show more efficient DNA condensing ability but lower DNA binding constants than **GV1**. However, the hydrophobic alkyl ether chains also enhance the DNA deliv-

ery ability of **GV2–6** compared with that of **GV1**. More importantly, we have applied **GV1–6** as non-viral gene vectors for tracking DNA delivery in living cells by one- and two-photon fluorescence microscopies. In two-photon microscopy, a high signal-to-noise contrast was achieved by irradiation with an 830 nm laser. This is the first example of the use of transition-metal complexes for two-photon luminescent tracking of the cellular pathways of gene delivery and as DNA carriers. Our work provides new insights into improving real-time tracking during gene delivery and transfection as well as important information for the design of multifunctional non-viral vectors.

## Introduction

Non-viral gene delivery systems have gained immense importance, primarily due to their in vivo safety compared to viral vectors.<sup>[1]</sup> However, the poor transfection efficiency of these vectors in vivo has impeded their development as therapeutics.<sup>[2]</sup> To achieve safe and efficient DNA delivery, a better understanding of the critical steps in the transfection process is necessary. Because non-viral vectors usually lack intrinsic fluorescence, they cannot be used to monitor the DNA delivery process (from transfection to release). The most commonly used method for intracellular plasmid trafficking is the fluorescent labeling of non-viral vectors with organic dyes.<sup>[3]</sup> To observe dynamic changes during a specific period of time (tracking), the dye must possess improved photostability and must be photostable under continual irradiation with light from fluorescent microscopes. However, most organic dyes have notable shortcomings, including poor solubility in water,

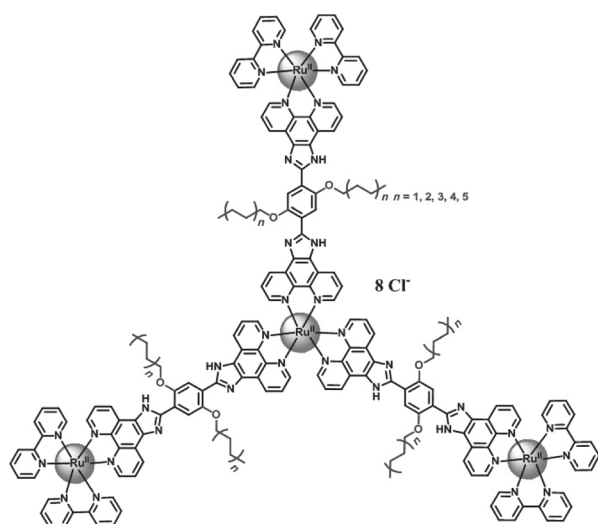
high toxicity to living cells, and poor photostability. Organic dyes may also cause extensive cellular damage and unwanted background signals due to the ultraviolet (UV) radiation required for their excitation and small Stokes shifts.<sup>[4]</sup> The short excitation wavelengths (< 650 nm) also preclude the use of these materials in thick tissues or live animals due to the associated low penetration depths.<sup>[5]</sup> In addition, the introduction of dyes may alter the delivery mechanism and lead to increased side-effects.<sup>[6]</sup> The use of chemical materials with intrinsic two-photon fluorescence as DNA carriers is an attractive solution to these problems because these molecules exhibit near-infrared (NIR) or longer excitation wavelengths, lower phototoxicity, greater penetration depths, and reduced photobleaching.<sup>[7]</sup> Therefore, the development of a two-photon fluorescent intracellular tracking vector will be valuable in the field of gene delivery.

Recently, the use of transition-metal complexes as luminescent probes has attracted increasing interest due to their advantageous photophysical properties.<sup>[8]</sup> More interestingly, some dinuclear ruthenium(II) complexes with low toxicity have been successfully used as two-photon luminescence probes for nuclear DNA staining,<sup>[9]</sup> cellular imaging,<sup>[10]</sup> and metal ion detection in living cells.<sup>[11]</sup> Based on these studies, multinuclear ruthenium(II) complexes have emerged as novel and promising candidates for two-photon luminescent imaging in living cells. Furthermore, several recent notable reports have shown that multinuclear complexes can effectively induce DNA condensation due to their greater variety of charge states and that they can serve as non-viral gene vectors.<sup>[12]</sup> These observations encouraged us to develop multinuclear ruthenium(II) complexes

[a] Dr. B. Yu, C. Ouyang, K. Qiu, Prof. L. Ji, Prof. H. Chao  
MOE Key Laboratory of Bioinorganic and Synthetic Chemistry  
School of Chemistry and Chemical Engineering  
Sun Yat-Sen University  
Guangzhou 510275 (P. R. China)  
E-mail: ceschh@mail.sysu.edu.cn

[b] Dr. B. Yu, Prof. J. Zhao  
School of Chemical Biology and Biotechnology  
Peking University  
Shenzhen 518055 (P. R. China).

Supporting information for this article is available on the WWW under <http://dx.doi.org/10.1002/chem.201405151>.



**Scheme 1.** Structures of **GV1** (without chains), **GV2** ( $n=1$ ), **GV3** ( $n=2$ ), **GV4** ( $n=3$ ), **GV5** ( $n=4$ ), and **GV6** ( $n=5$ ).

for use in two-photon luminescent tracking of the cellular pathways of gene delivery and as DNA carriers.

We have previously reported a tetranuclear ruthenium(II) complex  $[\text{Ru}\{\text{(bpy)}_2\text{Ru}(\text{H}_2\text{bpib})\}_3]\text{Cl}_8$  (**GV1**, Scheme 1;  $\text{H}_2\text{bpib} = 2,2'$ -*p*-phenylenebis(imidazo[4,5-*f*]phenanthroline)) as a one-photon luminescent non-viral gene vector for real-time tracking during delivery and transfection.<sup>[12d]</sup> Therefore, **GV1** was an ideal candidate for the further study and development of one- and two-photon luminescent tracking non-viral gene vectors. Moreover, the transfection efficiency of **GV1** was markedly improved in the presence of the neutral phospholipid DOPE (1,2-dioleoyl-*sn*-glycero-3-phosphoethanolamine). These findings indicated that the transfection efficiency of non-viral gene vectors can be improved by increasing the lipophilicity of the transfection systems. This observation prompted us to append alkyl ether chains of increasing length to the parent complex **GV1** to obtain five lipophilic tetranuclear ruthenium(II) complexes, **GV2–6** (Scheme 1). Herein, we demonstrate that this strategy is effective in improving the transfection efficiency of the parent complex **GV1** while preserving its rich photophysical properties. To the best of our knowledge, this is the first example of the use of transition-metal complexes as DNA carriers in combination with two-photon luminescent imaging to follow DNA intracellular trafficking with time.

## Results and Discussion

### Synthesis and characterization

The synthetic route to **GV2–6** is shown in Figure 1. We started with the respective 2,5-dialkoxyterephthalaldehydes (**1**), which were obtained according to methods described in the literature.<sup>[13]</sup> The 2,5-dialkoxyterephthalimidazo[4,5-*f*]phenanthroline ligands (**2**) were obtained in yields of 65–85% through condensation of 1,10-phenanthroline-5,6-dione with the respective 2,5-dialkoxyterephthalaldehydes at molar ratios of 2:1 in

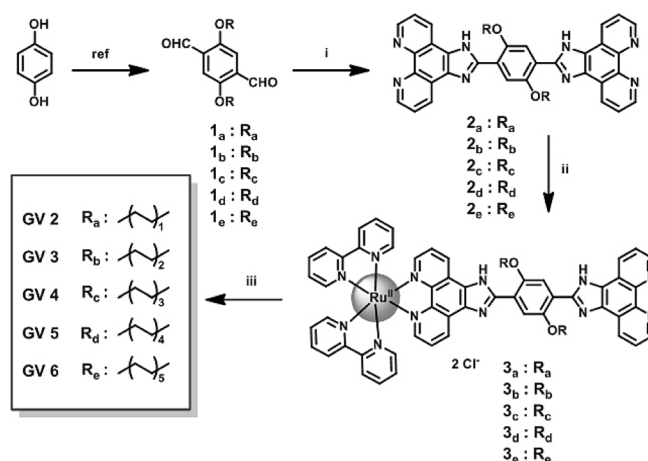


**Figure 1.** Synthetic route to **GV2–6**: (i) 1,10-phenanthroline-5,6-dione; (ii)  $[\text{Ru}(\text{bpy})_2\text{Cl}_2]$ ; (iii)  $[\text{Ru}(\text{DMSO})_4\text{Cl}_2]$ .

refluxing glacial acetic acid containing ammonium acetate. The mononuclear complexes **3** were prepared in yields of 63–74% by reactions of  $[\text{Ru}(\text{bpy})_2\text{Cl}_2]$  with ligands **2** in a 1:2 molar ratio in ethanol (DMF was utilized in the case of **3a** due to the low solubility of its ligand **2a** in ethanol). Reactions of  $[\text{Ru}(\text{DMSO})_4\text{Cl}_2]$  with three equivalents of each of the mononuclear complexes **3** in DMF produced the corresponding tetranuclear complexes **GV2–6** in yields of 75–87%. All of the complexes were purified by column chromatography and characterized by elemental analysis,  $^1\text{H}$  NMR, and ES-MS (Figures S1–S24 in the Supporting Information).

Next, we studied the electronic absorption and emission spectra of **GV1–6** in aqueous media (DMSO/ $\text{H}_2\text{O}$ , 1:99, v/v) at 298 K. All of the complexes showed good solubility. The energy maxima and absorption coefficients are summarized in Table S1 (see the Supporting Information). The spectra of **GV2–6** consist of three well-resolved bands at 287, 388, and 473 nm in the range 200–700 nm, with red shifts of approximately 9–15 nm for the latter two bands compared with those of **GV1** (Figure S25 in the Supporting Information). The bands at 287 and 388 nm can be attributed to the  $\pi\text{--}\pi^*$  (bpy) and  $\pi\text{--}\pi^*$  (bridging ligand **2**) intraligand transitions, respectively, based on comparison with the UV/Vis spectrum of  $[\text{Ru}(\text{bpy})_3]^{2+}$ . The lowest-energy band at 473 nm can be assigned to metal-to-ligand charge transfer (MLCT) and consists of overlapping  $\text{Ru}(\text{d}\pi)\text{--}2(\pi^*)$  and  $\text{Ru}(\text{d}\pi)\text{--}\text{bpy}(\pi^*)$  transitions. Excitation of the MLCT bands of **GV1–6** at room temperature results in a characteristic broad emission peak between 550 and 750 nm (Figure S26 in the Supporting Information). The emission maxima and relative quantum yields are presented in Table S1 (see the Supporting Information). Luminescence decay experiments performed at room temperature indicated lifetimes of **GV1–6** of 0.35–0.58  $\mu\text{s}$  by fitting the data to single-exponential decay functions.

The two-photon absorption (TPA) properties of **GV1–6** were also studied. With reference to Rhodamine B,<sup>[14]</sup> the largest two-photon absorption (TPA) cross-sections  $\delta$  of approximately 466–643 Göppert–Mayer (GM) units ( $1 \text{ GM} = 1 \times$

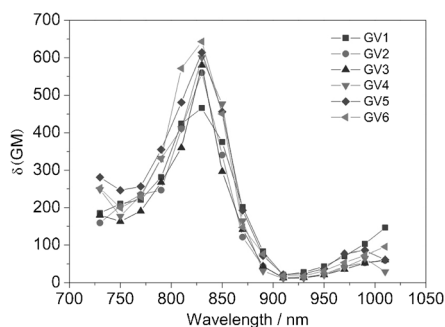


**Figure 2.** Two-photon-excited spectra of **GV1–6** at different excitation wavelengths from 730 to 1010 nm.

$10^{-50} \text{ cm}^4 \text{ s}^{-1} \text{ photon}^{-1}$ ) were measured at 830 nm (Figure 2 and Table S1 in the Supporting Information), which are hundreds of times larger than the TPA cross-sections of commercially available dyes for two-photon-excited (TPE) microscopy (0.16 GM for 4',6-diamidino-2-phenylindole (DAPI) and 1 GM for Cascade Blue fluorescent dyes<sup>[14a]</sup>) and also much higher than those of certain recently reported two-photon bio-available molecular probes.<sup>[9–11]</sup> The two-photon process was confirmed by power dependence experiments. A log-log linear relationship was observed between the emission intensity and the incident power, with slopes of 1.85 for **GV1**, 2.05 for **GV2**, 1.91 for **GV3**, 1.88 for **GV4**, 1.94 for **GV5**, and 1.83 for **GV6** (Figure S27 in the Supporting Information).

### DNA interactions

Preliminary evidence for the abilities of **GV1–6** to induce DNA condensation was obtained from electrophoresis mobility assays performed with plasmid pBR322 DNA. As shown in Figure 3, on increasing the concentrations of **GV1–6** (from 0 to

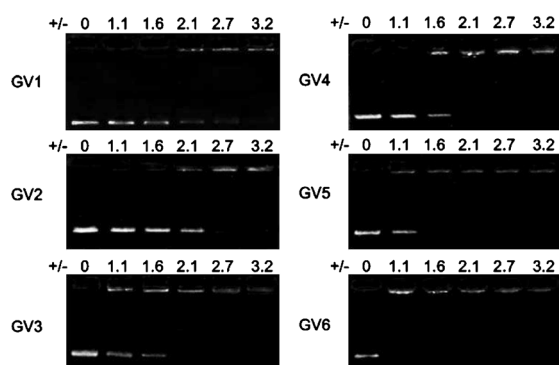


**Figure 3.** Agarose gel electrophoresis patterns of pBR322 DNA (7.5  $\mu\text{m}$ ) after incubation with **GV1–6** at various +/- ratios in aqueous solution.

6  $\mu\text{m}$ ), the amount of supercoiled, closed circular pBR322 DNA (7.5  $\mu\text{m}$  each well) gradually diminished, and retardation of the DNA in the gel well became increasingly obvious. **GV1** showed obvious condensation effects on DNA until the concentration reached a +/- ratio (total positive charge/total negative charge) of 3.2. **GV2–6**, bearing hydrophobic chains, completely

condensed DNA at lower +/- ratios (2.7 for **GV2**, 2.1 for **GV3**, 2.1 for **GV4**, 1.6 for **GV5**, and 1.1 for **GV6**). The results indicated that the introduction of alkyl ether chains on **GV1** enhanced the DNA condensing ability of complexes **GV2–6**, even in the case of complex **GV2** with only four-carbon chains.

We investigated the DNA binding abilities of **GV1–6** through a DNA (calf thymus DNA) titration approach. The DNA binding constant of **GV1** was  $1.46 \times 10^6 \text{ M}^{-1}$ , whereas those of **GV2–6** were measured as  $1.88\text{--}8.66 \times 10^5 \text{ M}^{-1}$  (Figure S28 in the Supporting Information). The DNA binding constants of these complexes are much larger than those of dinuclear  $\text{Ru}^{\text{II}}$  complexes that do not intercalate DNA, such as  $[\text{Ru}_2(\text{TBphen}_2)(\text{bpy})_4]^{4+}$  (TBPhen2 = bis-phenanthroline) ( $4.85 \times 10^3 \text{ M}^{-1}$ ) and  $[\text{Ru}_2(\text{TBphen}_2)(\text{phen})_4]^{4+}$  ( $9.11 \times 10^4 \text{ M}^{-1}$ ),<sup>[15]</sup> but comparable to those of typical DNA intercalative dinuclear  $\text{Ru}^{\text{II}}$  complexes, such as  $[\text{Ru}_2(\text{bdptb})(\text{bpy})_4]^{4+}$  ( $7.60 \times 10^5 \text{ M}^{-1}$ ; bdptb = 2,2'-bis(5,6-diphenyl-1,2,4-triazin-3-yl)-4,4'-bipyridine)<sup>[16]</sup> and  $[\text{Ru}_2(\text{bmbh})(\text{dpq})_4]^{4+}$  ( $3.60 \times 10^6 \text{ M}^{-1}$ ; bmbh = 1,7-bis(4'-methyl-2,2'-bipyridin-4-yl)heptane, dpq = pyrazino[2,3-f][1,10]phenanthroline).<sup>[17]</sup> The results indicated that in addition to the electrostatic interaction between the complexes and DNA, there was also an intermolecular  $\pi\text{--}\pi$  interaction between the bridging ligand and the DNA base pairs. Moreover, the hydrophobic chains on the bridging ligands could weaken this intermolecular  $\pi\text{--}\pi$  interaction. This phenomenon was also evident from zeta potential measurements by dynamic light scattering (DLS).

We determined the zeta potentials of **GV1–6**-pBR322 DNA particles at various +/- ratios in aqueous solution. As shown in Figure 4a, overall, the zeta potentials of **GV1–6**-DNA particles increased with increasing +/- ratios. At the same +/- ratio, the zeta potentials of **GV1**-DNA particles were stronger

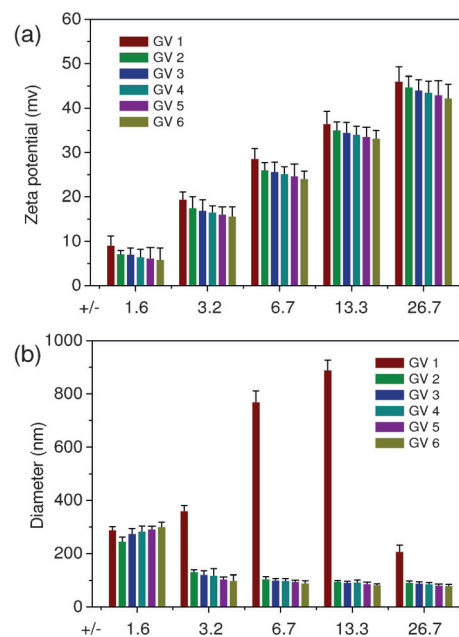


**Figure 4.** (a) Zeta potentials and (b) hydrodynamic diameters of pBR322 DNA (1.5  $\mu\text{m}$ ) incubated with **GV1–6** at various +/- ratios in aqueous solution.

than those of **GV2-6**. Small decreases for the complexes with longer chains were observed at all  $+/-$  ratios. The results also indicated that complexes with longer chains had weaker DNA binding abilities. However, for DNA condensation, the hydrophobic effect and electrostatic interaction were apparently more important.

We investigated the DNA binding and condensing behaviors of the complexes in aqueous solution based on the size of the **GV1-6-pBR322** DNA particles at various  $+/-$  ratios determined by DLS. With increasing  $+/-$  ratio from 1.6 to 13.3, the hydrodynamic diameter of the **GV1**-DNA particles increased from 300 to 900 nm due to low thermal dynamic stability. When the  $+/-$  ratio was 26.7 or higher,<sup>[12d]</sup> the **GV1**-DNA particles had higher thermal dynamic stability with an average size of approximately 200 nm. Although the DNA binding ability of **GV1** is stronger than those of **GV2-6**, **GV2-6**-DNA particles showed thermal dynamic stability at a much lower  $+/-$  ratio of 6.7, with diameters of approximately 100 nm (Figure 4b). The results indicated no obvious correlation between the DNA binding and condensing abilities and the size of the DNA particles, although **GV2-6** bearing hydrophobic alkyl ether chains exhibited more efficient DNA condensing ability in aqueous solution than **GV1**. Moreover, the thermal dynamic stability of DNA particles ( $+/-$  ratios of 26.7 for **GV1**, 6.7 for **GV2-6**) was important for subsequent studies (AFM, cellular uptake, transfection, cytotoxicity).

AFM was employed to further elucidate the formation and morphology of the DNA particles. In the absence of  $\text{Ru}^{\text{II}}$  complexes, the free DNA existed as loose clews or relaxed circles, with little twisting of the strands (Figure 5). This structure is characteristic of uncondensed DNA morphology.<sup>[18]</sup> After mixing the  $\text{Ru}^{\text{II}}$  complexes with pBR322 DNA, DNA particles were formed. As in our previous study,<sup>[12d]</sup> **GV1** showed well-distributed DNA particles from 100 to 200 nm at a  $+/-$  ratio of 26.7. In contrast, **GV2-6**-DNA particles with sizes of approximately 30–60 nm were found in freshly cleaved mica at a lower  $+/-$  ratio of 6.7, and small particles of approximately 10 nm were also observed (Figure 5).

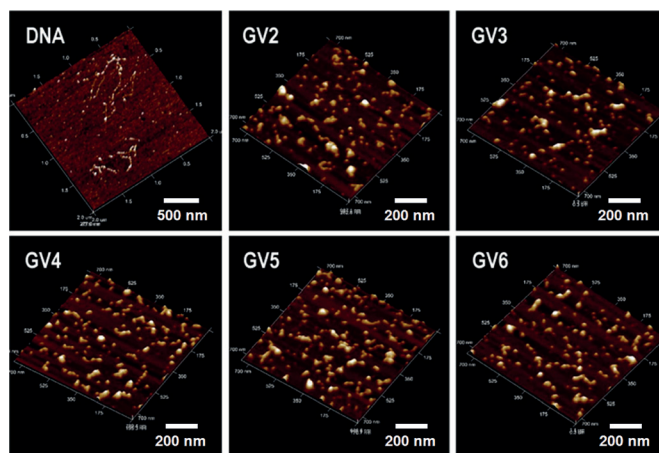


**Figure 5.** AFM images of pBR322 DNA (1.5  $\mu\text{M}$ ) in the absence or presence of complexes **GV2-6** at a  $+/-$  ratio of 6.7.

Gene vectors are known to protect pDNA against nuclease-catalyzed biodegradation. Therefore, **GV1-pBR322** DNA particles at a  $+/-$  ratio of 26.7 and **GV2-6-pBR322** DNA particles at a  $+/-$  ratio of 6.7 were incubated with DNase-I (Figure S29 in the Supporting Information). After DNase-I degradation, DNA from the particles should migrate approximately the same distance as the control DNA under a fixed electric field. However, compared with naked pDNA, no DNA bands for DNase-I digestion were observed with the ruthenium(II) complex-bound DNA particles. These results indicated that **GV1-6** can protect DNA from DNase degradation. We also performed DNA photodamage experiments in the presence of **GV1-6**. DNA photocleavage assays (Figure S30 in the Supporting Information) and continuous irradiation experiments (Figure S31 in the Supporting Information) showed that despite their high affinity for DNA, **GV1-6** displayed no photocleavage effects or photoreactivity towards DNA.

### Cellular uptake of DNA particles

High DNA uptake level is a prerequisite for efficient gene transfection. Flow cytometry was used to quantify the uptake of **GV1-6-pEGFP** DNA particles in HeLa cells. Figure 6 shows flow

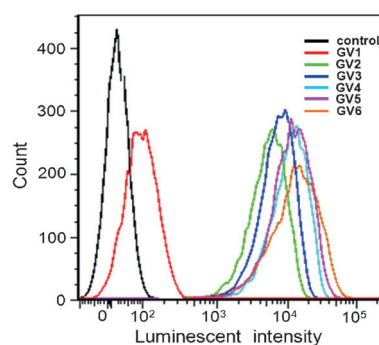


**Figure 6.** Quantitative flow cytometry results shown as fluorescence intensities of HeLa cells incubated with **GV1-6-pEGFP** DNA particles for 4 h. The DNA concentration was 1.5  $\mu\text{M}$ . **GV1-pEGFP** DNA particles at a  $+/-$  ratio of 26.7 and **GV2-6-pEGFP** DNA particles at a  $+/-$  ratio of 6.7. Untreated cells served as a control.

cytometry results for HeLa cells incubated with **GV1-6**-DNA particles and for untreated cells as a control. Based on the average fluorescence intensities of the cells, **GV2-6** obviously facilitated greatly enhanced intracellular delivery of DNA compared with **GV1**. A previous report<sup>[19]</sup> indicated that the internalization of 50–100 nm DNA particles (the size of **GV2-6**-DNA particles) by endocytosis is two- to ten-fold more efficient than that of 200 nm particles (the size of **GV1**-DNA particles). According to quantitative analysis, cellular uptake of **GV2-6**-DNA particles was enhanced 50- to 120-fold compared with that of **GV1**. By increasing the length of the alkyl chains, the average fluorescence intensity of the cells was also enhanced. These results indicated that the hydrophobic effect played the most important role in the cellular uptake of DNA particles in our study.

We further examined the localization of these DNA particles in HeLa cells by TEM. In a previous study,<sup>[12d]</sup> **GV1**-DNA particles were found in the endosomes and cytoplasm of HeLa cells. In this study, some **GV2-6**-DNA particles were observed on the cell membrane due to their lipophilicity, and some were observed in the endosome or cytoplasm as a result of endocytosis pathways in HeLa cells (Figure 7 and Figure S32 in the Supporting Information). The DNA particle size was approximately 50 nm. Moreover, with increasing chain length, more DNA particles entered the HeLa cells, based on the flow cytometry results.

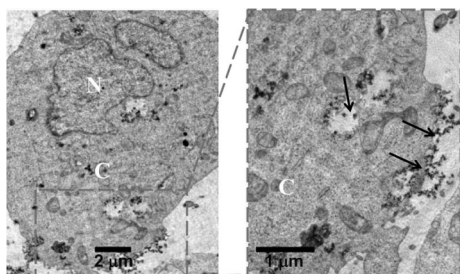


**Figure 7.** Cellular uptake and intracellular localization of **GV2**-pEGFP DNA particles at a  $+/-$  ratio of 6.7 monitored by TEM (N: nucleus, C: cytoplasm). The locations of DNA particles are indicated by black arrows.

### Transfection and imaging

To investigate the intracellular behaviors of **GV1-6**-pEGFP DNA particles, one- and two-photon fluorescence microscopies were used to monitor the time-dependent transport and transfection of pEGFP DNA plasmids condensed by these complexes. We stained the nuclei of the HeLa cells with Hoechst 33258, and then the DNA particles were added. The DNA condensed by **GV1** was found throughout the entire cell within 1 h, and its accumulation in the nucleus was observed after 4 h. The transport behavior of DNA condensed by **GV2-6** was different from that of DNA condensed by **GV1** (Figure 8 and Figures S33–S37 in the Supporting Information). The **GV2-6**-pEGFP DNA particles were attached to the cell membrane after 1 h. Additional accumulation of DNA at the cell membrane was observed, and some DNA had entered the cytoplasm after 4 h. The culture medium was then replaced with fresh DMEM containing 10% fetal bovine serum (FBS). After a further 12 h with these complexes, EGFP expression was detected, and higher EGFP expression was observed after 24 h. Similar behaviors were observed under one-photon and two-photon excitation. In addition, due to the two-photon absorption, the background signal was strongly suppressed, and a higher resolution image was obtained using two-photon confocal laser scanning microscopy.

We determined the relative transfection efficiency of this non-viral system based on luciferase assays, and the pGL3 plasmid was used as a control vector (Figure S38 in the Supporting Information). Multiple experiments on HeLa cells showed the relative luminescence intensity (RLU) from the oxidized luciferin of  $10^4$  cells. For the control (DNA alone), the luciferase

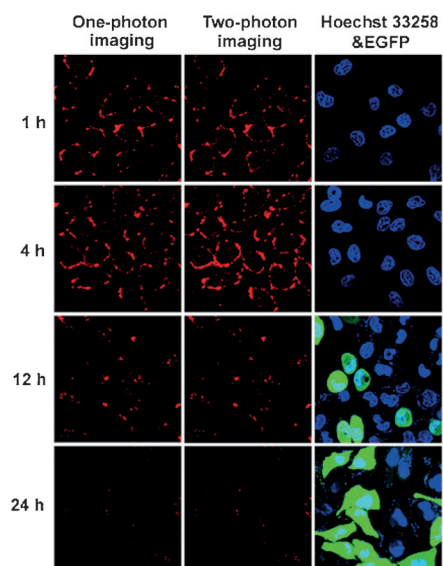


**Figure 8.** Time-dependent confocal microscopy images of the entry and transportation of **GV4**-pEGFP DNA particles at a  $+/-$  ratio of 6.7 in HeLa cells. The red luminescence is due to **GV4** and the blue and green fluorescences are due to Hoechst 33258 and EGFP, respectively.

expression was low. The luciferase expression increased when **GV1-6** were used. With the hydrophobic chains, the transfection efficiencies of **GV2-6** were clearly improved 10- to 20-fold compared with that of **GV1**. On increasing the length of the chains, the transfection efficiencies of the complexes increased for **GV2-5** but decreased in the case of **GV6**. Moreover, when we introduced the neutral phospholipid DOPE into these transfection systems, the transfection efficiencies of **GV2-6** exhibited small decreases, except in the case of **GV1**. We believe this finding to be related to the cytotoxicity of the transfection systems (see below).

### Cytotoxicity

The cytotoxicity of non-viral gene vectors is one of the major concerns in gene delivery. Therefore, we examined the viability of HeLa cells treated with these transfection systems. As shown in Figure S39 (see the Supporting Information), overall, the cytotoxicities of **GV1-6**-pEGFP DNA particles (–) exhibited small increases compared with **GV1-6** alone (o). With DOPE (+), the viability of the HeLa cells clearly decreased in the presence of **GV1-6**-pEGFP DNA particles. By increasing the length of the chains, the cytotoxicities of **GV2-6** and the transfection systems increased. Among these transfection systems, DNA particles with **GV1** exhibited the highest cytotoxicity at high concentrations and high  $+/-$  ratios. The viability of HeLa cells with these transfection systems (without DOPE) was higher than 70%. The results indicated that our transfection system exhibited relatively low cytotoxicity.

### Conclusion

We have designed and synthesized five new lipophilic tetranuclear ruthenium(II) complexes, **GV2-6**, based on the parent

complex **GV1**. With hydrophobic alkyl ether chains, **GV2–6** exhibited more efficient DNA condensing abilities in aqueous solution and better cellular uptake capacities than **GV1**. The hydrophobic alkyl ether chains also enhanced their DNA delivery abilities and transfection efficiencies compared with those of **GV1**. More interestingly, we have demonstrated for the first time that transition-metal complexes can be used as two-photon luminescent tracking non-viral gene vectors in living cells. This study provides information regarding improvements of real-time tracking during gene delivery and transfection and the design of multifunctional non-viral vectors.

## Experimental Section

### Materials and general instruments

Ethidium bromide (EB), 4',6-diamidino-2-phenylindole (DAPI), 1,2-dioleoyl-*sn*-glycero-3-phosphoethanolamine (DOPE), 3-(4,5-dimethylthiazol-2-yl)-2,5-diphenyltetrazolium bromide (MTT), and calf thymus DNA (CT-DNA) were purchased from Sigma. Plasmid pBR322 DNA was obtained from MBI Fermentas, plasmid pEGFP DNA from Clontech, and plasmid pGL3 control vector and luciferase kit from Promega. Unless otherwise stated, DNA concentration is expressed in terms of base pairs. All samples were prepared using distilled water that had been passed through a Millipore-Q ultra-purification system.

Microanalysis (C, H, and N) was carried out with a Vario EL cube elemental analyzer. <sup>1</sup>H NMR spectra were recorded on Varian Mercury Plus 300 or Bruker AVANCE IIIIT 600HD spectrometers at 25 °C. All chemical shifts are given relative to tetramethylsilane (TMS). Fast atom bombardment mass spectra (FAB-MS) were acquired on a VG ZAB-HS spectrometer from samples in a 3-nitrobenzyl alcohol matrix. Electrospray mass spectra (ES-MS) were recorded on an LCQ system (Finnigan MAT, USA). UV/Vis spectra were recorded on a Perkin-Elmer Lambda 850 spectrophotometer. Emission spectra were recorded on a Perkin-Elmer LS 55 spectrofluorophotometer at room temperature (25 °C). Time-resolved emission measurements were conducted on an FLS 920 combined fluorescence-lifetime and steady-state spectrometer. Quantum yields of luminescence at room temperature (25 °C) were calculated according to literature procedures, by using an aerated aqueous solution of [Ru(bpy)<sub>3</sub>]<sup>2+</sup> ( $\phi = 0.028$ )<sup>[8a]</sup> as the reference emitter. All data were processed using the Origin Pro 7.5 software package.

### Synthesis

The respective 2,5-dialkoxyterephthalaldehydes (**1a–1e**)<sup>[13]</sup>, 1,10-phenanthroline-5,6-dione, [Ru(bpy)<sub>3</sub>Cl<sub>2</sub>] $\cdot$ 2H<sub>2</sub>O, [Ru(DMSO)<sub>4</sub>Cl<sub>2</sub>], and [Ru{(bpy)<sub>2</sub>Ru(H<sub>2</sub>bpiib)}<sub>3</sub>]<sub>3</sub>Cl<sub>8</sub> (**GV1**) were synthesized according to literature methods.<sup>[12d]</sup>

**Synthesis of 2,5-dibutoxyterephthalimidazo[4,5-f]phenanthroline (2a):** A mixture of 1,10-phenanthroline-5,6-dione (0.21 g, 1 mmol), ammonium acetate (1.55 g, 20 mmol), **1a** (0.139 g, 0.5 mmol), and glacial acetic acid (20 mL) was heated under reflux for about 4 h and then cooled to room temperature. On adding water (60 mL), a precipitate was formed, which was collected and washed with water. The crude product was recrystallized from ethanol and produced a greenish-yellow powder. Yield: 0.28 g, 85.1%; elemental analysis calcd (%) for C<sub>40</sub>H<sub>34</sub>N<sub>8</sub>O<sub>2</sub>: C 72.93, H 5.20, N 17.01; found: C 74.97, H 5.17, N 16.96; FAB-MS: *m/z*: 659 [M+1]. The compound is only sparingly soluble in organic solvents such as DMF and DMSO, and so <sup>1</sup>H NMR data could not be obtained.

**Synthesis of 2,5-dihexoxyterephthalimidazo[4,5-f]phenanthroline (2b):** Ligand **2b** was synthesized in a manner identical to that described for **2a**, except with **1b** (0.167 g, 0.5 mmol) in place of **1a**. Yield: 0.29 g, 81.2%; elemental analysis calcd (%) for C<sub>40</sub>H<sub>34</sub>N<sub>8</sub>O<sub>2</sub>: C 73.93, H 5.92, N 15.67; found: C 74.02, H 5.85, N 15.58; <sup>1</sup>H NMR (300 MHz, [D<sub>6</sub>]DMSO):  $\delta = 13.20$  (s, 2H), 9.04–8.96 (m, 8H), 8.00 (s, 2H), 7.85 (q, *J*<sub>1</sub> = 6 Hz, *J*<sub>2</sub> = 3 Hz, 4H), 4.32 (t, *J* = 5 Hz, 4H), 1.97–1.89 (m, 4H), 1.45–1.39 (m, 4H), 1.27–1.23 (m, 4H), 1.16–1.13 (m, 4H), 0.66 ppm (t, *J* = 7.5 Hz, 6H); FAB-MS: *m/z*: 715 [M+1].

**Synthesis of 2,5-dioctoxyterephthalimidazo[4,5-f]phenanthroline (2c):** Ligand **2c** was synthesized in a manner identical to that described for **2a**, except with **1c** (0.195 g, 0.5 mmol) in place of **1a**. Yield: 0.30 g, 78.0%; elemental analysis calcd (%) for C<sub>40</sub>H<sub>34</sub>N<sub>8</sub>O<sub>2</sub>: C 74.78, H 6.54, N 14.53; found: C 74.85, H 6.46, N 14.50; <sup>1</sup>H NMR (300 MHz, [D<sub>6</sub>]DMSO):  $\delta = 13.22$  (s, 2H), 9.04–8.96 (m, 8H), 8.00 (s, 2H), 7.84 (q, *J*<sub>1</sub> = 6 Hz, *J*<sub>2</sub> = 3 Hz, 4H), 4.33 (t, *J* = 5 Hz, 4H), 1.96–1.87 (m, 4H), 1.43–1.39 (m, 4H), 1.26–1.23 (m, 4H), 0.98–0.94 (m, 20H), 0.67 ppm (t, *J* = 7.5 Hz, 6H); FAB-MS: *m/z*: 771 [M+1].

**Synthesis of 2,5-didecoxyterephthalimidazo[4,5-f]phenanthroline (2d):** Ligand **2d** was synthesized in a manner identical to that described for **2a**, except with **1d** (0.223 g, 0.5 mmol) in place of **1a**. Yield: 0.30 g, 72.6%; elemental analysis calcd (%) for C<sub>40</sub>H<sub>34</sub>N<sub>8</sub>O<sub>2</sub>: C 75.51, H 7.07, N 13.55; found: C 75.64, H 6.98, N 13.51; <sup>1</sup>H NMR (300 MHz, [D<sub>6</sub>]DMSO):  $\delta = 13.21$  (s, 2H), 9.03–8.95 (m, 8H), 8.00 (s, 2H), 7.82 (q, *J*<sub>1</sub> = 3 Hz, *J*<sub>2</sub> = 6 Hz, 4H), 4.33 (t, *J* = 5 Hz, 4H), 1.96–1.87 (m, 4H), 1.43–1.39 (m, 4H), 1.27–1.22 (m, 4H), 1.04–0.90 (m, 20H), 0.58 ppm (t, *J* = 7.5 Hz, 6H); FAB-MS: *m/z*: 827 [M+1].

**Synthesis of 2,5-didodecoxyterephthalimidazo[4,5-f]phenanthroline (2e):** Ligand **2e** was synthesized in a manner identical to that described for **2a**, except with **1e** (0.195 g, 0.5 mmol) in place of **1a**. Yield: 0.29 g, 65.8%; elemental analysis calcd (%) for C<sub>40</sub>H<sub>34</sub>N<sub>8</sub>O<sub>2</sub>: C 76.16, H 7.53, N 12.69; found: C 76.03, H 7.67, N 12.62; <sup>1</sup>H NMR (300 MHz, [D<sub>6</sub>]DMSO):  $\delta = 9.04$ –8.91 (m, 8H), 8.01 (s, 1H), 7.80 (q, *J*<sub>1</sub> = 8 Hz, *J*<sub>2</sub> = 10 Hz, 4H), 7.64 (s, 1H), 4.12 (t, *J* = 7.5 Hz, 2H), 4.01 (t, *J* = 7.5 Hz, 2H), 1.96–1.71 (m, 8H), 1.23–0.77 ppm (m, 38H); FAB-MS: *m/z*: 883 [M+1].

**Synthesis of [Ru(bpy)<sub>2</sub>(2a)Cl<sub>2</sub>] (3a):** Ligand **2a** (0.165 g, 0.25 mmol) was first dissolved in hot DMF (20 mL), then [Ru(bpy)<sub>2</sub>Cl<sub>2</sub>] $\cdot$ 2H<sub>2</sub>O (0.065 g, 0.125 mmol) was added and the mixture was heated under reflux for 12 h to give a clear red solution. After removal of the solvent in a rotary evaporator, the red product was purified by column chromatography on alumina eluting with acetonitrile/ethanol (10:1, v/v) and dried in vacuo. Yield: 0.090 g, 63.1%; elemental analysis calcd (%) for C<sub>60</sub>H<sub>50</sub>Cl<sub>2</sub>N<sub>12</sub>O<sub>2</sub>Ru: C 63.04, H 4.41, N 14.70; found: C 63.12, H 4.37, N 14.61; <sup>1</sup>H NMR (300 MHz, [D<sub>6</sub>]DMSO):  $\delta = 9.18$ –8.84 (m, 10H), 8.20 (t, *J* = 9 Hz, 2H), 8.10 (t, *J* = 7.5 Hz, 2H), 8.00–7.83 (m, 10H), 7.58 (t, *J* = 10.5 Hz, 4H), 7.35 (t, *J* = 6 Hz, 2H), 4.32 (t, *J* = 6 Hz, 4H), 1.97–1.85 (m, 4H), 1.57–1.44 (m, 4H), 0.91 ppm (q, *J*<sub>1</sub> = *J*<sub>2</sub> = 9 Hz, 6H); MS (ESI, CH<sub>3</sub>OH): *m/z*: 357.7 ([M–2Cl+H]<sup>3+</sup>), 535.3 ([M–2Cl]<sup>2+</sup>), 713.4 ([2M–4Cl–H]<sup>3+</sup>), 1071.3 ([M–2Cl–H]<sup>+</sup>).

**Synthesis of [Ru(bpy)<sub>2</sub>(2b)Cl<sub>2</sub>] (3b):** Ligand **2b** (0.179 g, 0.25 mmol) was first dissolved in hot ethanol (20 mL), then [Ru(bpy)<sub>2</sub>Cl<sub>2</sub>] $\cdot$ 2H<sub>2</sub>O (0.065 g, 0.125 mmol) was added and the mixture was heated under reflux for 8 h to give a clear red solution. After removal of the solvent in a rotary evaporator, the red product was purified by column chromatography on alumina eluting with acetonitrile/ethanol (8:1, v/v) and dried in vacuo. Yield: 0.100 g, 66.7%; elemental analysis calcd (%) for C<sub>64</sub>H<sub>58</sub>Cl<sub>2</sub>N<sub>12</sub>O<sub>2</sub>Ru: C 64.10, H 4.87, N 14.02; found: C 64.18, H 4.77, N 13.96; <sup>1</sup>H NMR (300 MHz, [D<sub>6</sub>]DMSO):  $\delta = 9.15$ –8.84 (m, 10H), 8.20 (t, *J* = 9 Hz, 2H), 8.10 (t, *J* =

7.5 Hz, 2H), 7.97–7.81 (m, 10H), 7.58 (d,  $J=9$  Hz, 4H), 7.35 (t,  $J=6$  Hz, 2H), 4.32 (t,  $J=7.5$  Hz, 4H), 1.96–1.87 (m, 4H), 1.44–1.14 (m, 12H), 0.63 ppm (q,  $J_1=6$  Hz,  $J_2=9$  Hz, 6H); MS (ESI, CH<sub>3</sub>OH):  $m/z$ : 376.1 ([ $M-2Cl+H$ ]<sup>3+</sup>), 563.4 ([ $M-2Cl$ ]<sup>2+</sup>), 750.9 ([ $2M-4Cl-H$ ]<sup>3+</sup>), 1125.8 ([ $M-2Cl-H$ ]<sup>+</sup>).

**Synthesis of [Ru(bpy)<sub>2</sub>(2c)]Cl<sub>2</sub> (3c):** Complex **3c** was synthesized in a manner identical to that described for **3b**, except with **2c** (0.193 g, 0.25 mmol) in place of **2b**. Yield: 0.110 g, 70.5%; elemental analysis calcd (%) for C<sub>68</sub>H<sub>66</sub>Cl<sub>2</sub>N<sub>12</sub>O<sub>2</sub>Ru: C 65.06, H 5.30, N 13.39; found: C 64.18, H 5.67, N 13.56; <sup>1</sup>H NMR (300 MHz, [D<sub>6</sub>]DMSO):  $\delta=9.14$ – $8.84$  (m, 10H), 8.21 (t,  $J=7.5$  Hz, 2H), 8.10 (t,  $J=7.5$  Hz, 2H), 7.97–7.81 (m, 10H), 7.59 (q,  $J_1=3$  Hz,  $J_2=9$  Hz, 4H), 7.36 (t,  $J=6$  Hz, 2H), 4.29 (t,  $J=7.5$  Hz, 4H), 1.96–1.82 (m, 4H), 1.42–1.38 (m, 4H), 1.26–1.23 (m, 4H), 1.05–0.98 (m, 12H), 0.57 ppm (t,  $J=7.5$  Hz, 6H); MS (ESI, CH<sub>3</sub>OH):  $m/z$ : 592.6 ([ $M-2Cl$ ]<sup>2+</sup>).

**Synthesis of [Ru(bpy)<sub>2</sub>(2d)]Cl<sub>2</sub> (3d):** Complex **3d** was synthesized in a manner identical to that described for **3b**, except with **2d** (0.207 g, 0.25 mmol) in place of **2b**. Yield: 0.120 g, 73.3%; elemental analysis calcd (%) for C<sub>72</sub>H<sub>74</sub>Cl<sub>2</sub>N<sub>12</sub>O<sub>2</sub>Ru: C 65.94, H 5.69, N 12.82; found: C 66.03, H 5.61, N 12.76; <sup>1</sup>H NMR (300 MHz, [D<sub>6</sub>]DMSO):  $\delta=9.16$ – $8.84$  (m, 10H), 8.20 (t,  $J=7.5$  Hz, 2H), 8.10 (t,  $J=9$  Hz, 2H), 7.98–7.79 (m, 10H), 7.60 (t,  $J=4.5$  Hz, 4H), 7.35 (t,  $J=6$  Hz, 2H), 4.30 (t,  $J=4.5$  Hz, 4H), 1.92–1.85 (m, 4H), 1.46–0.90 (m, 28H), 0.66 ppm (t,  $J=7.5$  Hz, 6H); MS (ESI, CH<sub>3</sub>OH):  $m/z$ : 413.0 ([ $M-2Cl+H$ ]<sup>3+</sup>), 620.0 ([ $M-2Cl$ ]<sup>2+</sup>), 826.0 ([ $2M-4Cl-H$ ]<sup>3+</sup>), 1240.0 ([ $M-2Cl-H$ ]<sup>+</sup>).

**Synthesis of [Ru(bpy)<sub>2</sub>(2e)]Cl<sub>2</sub> (3e):** Complex **3e** was synthesized in a manner identical to that described for **3b**, except with **2e** (0.221 g, 0.25 mmol) in place of **2b**. Yield: 0.127 g, 74.2%; elemental analysis calcd (%) for C<sub>76</sub>H<sub>82</sub>Cl<sub>2</sub>N<sub>12</sub>O<sub>2</sub>Ru: C 66.75, H 6.04, N 12.29; found: C 66.83, H 5.97, N 12.21; <sup>1</sup>H NMR (300 MHz, [D<sub>6</sub>]DMSO):  $\delta=9.18$ – $8.85$  (m, 10H), 8.20 (t,  $J=7.5$  Hz, 2H), 8.10 (t,  $J=9$  Hz, 2H), 7.99–7.78 (m, 10H), 7.59 (q,  $J_1=6$  Hz,  $J_2=9$  Hz, 4H), 7.36 (t,  $J=6$  Hz, 2H), 4.29 (t,  $J=15$  Hz, 4H), 1.94–1.83 (m, 4H), 1.45–0.73 ppm (m, 40H); MS (ESI, CH<sub>3</sub>OH):  $m/z$ : 432.7 ([ $M-2Cl+H$ ]<sup>3+</sup>), 647.8 ([ $M-2Cl$ ]<sup>2+</sup>), 863.8 ([ $2M-4Cl-H$ ]<sup>3+</sup>).

**Synthesis of {[Ru(bpy)<sub>2</sub>(2a)]<sub>3</sub>Ru}Cl<sub>8</sub> (GV2):** A mixture of **3a** (0.114 g, 1 mmol), [Ru(DMSO)<sub>2</sub>Cl<sub>2</sub>] (0.016 g, 0.33 mmol), and DMF (5 mL) was heated under reflux under argon overnight. After evaporation of the solvent under reduced pressure, the product was purified by cation-exchange chromatography on SP-Sephadex C-25 eluting with a 0.5 M solution of NaCl in water/acetone (5:1, v/v). Yield: 0.090 g, 75.8%; elemental analysis calcd (%) for C<sub>180</sub>H<sub>150</sub>Cl<sub>8</sub>N<sub>36</sub>O<sub>6</sub>Ru<sub>4</sub>: C 60.03, H 4.20, N 14.00; found: C 59.83, H 4.58, N 13.75; <sup>1</sup>H NMR (600 MHz, [D<sub>6</sub>]DMSO):  $\delta=9.22$  (d,  $J=12$  Hz, 12H), 8.92 (d,  $J=18$  Hz, 12H), 8.23–7.79 (m, 48H), 7.61 (d,  $J=6$  Hz, 12H), 7.38 (t,  $J=12$  Hz, 6H), 4.31 (s, 12H), 1.90 (m, 12H), 1.56 (m, 12H), 0.94 ppm (t,  $J=12$  Hz, 18H); MS (ESI, CH<sub>3</sub>OH):  $m/z$ : 473.3 ([ $M-8Cl-H$ ]<sup>7+</sup>), 552.6 ([ $M-8Cl-2H$ ]<sup>6+</sup>), 662.6 ([ $M-8Cl-3H$ ]<sup>5+</sup>), 828.5 ([ $M-8Cl-4H$ ]<sup>4+</sup>).

**Synthesis of {[Ru(bpy)<sub>2</sub>(2b)]<sub>3</sub>Ru}Cl<sub>8</sub> (GV3):** Complex **GV3** was synthesized in a manner identical to that described for **GV2**, except with **3b** (0.120 g, 1 mmol) in place of **3a**. Yield: 0.095 g, 76.6%; elemental analysis calcd (%) for C<sub>192</sub>H<sub>174</sub>Cl<sub>8</sub>N<sub>36</sub>O<sub>6</sub>Ru<sub>4</sub>: C 61.18, H 4.65, N 13.38; found: C 61.24, H 4.58, N 13.25; <sup>1</sup>H NMR (600 MHz, [D<sub>6</sub>]DMSO):  $\delta=9.15$  (d,  $J=24$  Hz, 12H), 8.88 (t,  $J=24$  Hz, 12H), 8.24–7.79 (m, 48H), 7.63 (t,  $J=15$  Hz, 12H), 7.37 (t,  $J=12$  Hz, 6H), 4.32 (t,  $J=24$  Hz, 12H), 1.93 (m, 12H), 1.45–1.12 (m, 36H), 0.66 (t,  $J=6$  Hz, 9H), 0.56 ppm (t,  $J=9$  Hz, 9H); MS (ESI, CH<sub>3</sub>OH):  $m/z$ : 580.6 ([ $M-8Cl-2H$ ]<sup>6+</sup>), 696.6 ([ $M-8Cl-3H$ ]<sup>5+</sup>), 870.2 ([ $M-8Cl-4H$ ]<sup>4+</sup>).

**Synthesis of {[Ru(bpy)<sub>2</sub>(2c)]<sub>3</sub>Ru}Cl<sub>8</sub> (GV4):** Complex **GV4** was synthesized in a manner identical to that described for **GV2**, except with **3c** (0.126 g, 1 mmol) in place of **3a**. Yield: 0.101 g, 77.7%; elemental analysis calcd (%) for C<sub>204</sub>H<sub>198</sub>Cl<sub>8</sub>N<sub>36</sub>O<sub>6</sub>Ru<sub>4</sub>: C 62.22, H 5.07, N 12.80; found: C 62.34, H 5.01, N 12.74; <sup>1</sup>H NMR (600 MHz, [D<sub>6</sub>]DMSO):  $\delta=9.21$  (m, 12H), 8.88 (t,  $J=24$  Hz, 12H), 8.23–7.79 (m, 48H), 7.61 (t,  $J=12$  Hz, 12H), 7.36 (t,  $J=12$  Hz, 6H), 4.35 (t,  $J=24$  Hz, 12H), 1.93 (m, 12H), 1.45–1.07 (m, 60H), 0.44 ppm (m, 18H); MS (ESI, CH<sub>3</sub>OH):  $m/z$ : 522.2 ([ $M-8Cl-H$ ]<sup>7+</sup>), 609.4 ([ $M-8Cl-2H$ ]<sup>6+</sup>), 729.9 ([ $M-8Cl-3H$ ]<sup>5+</sup>), 912.1 ([ $M-8Cl-4H$ ]<sup>4+</sup>), 1217.2 ([ $M-8Cl-5H$ ]<sup>3+</sup>).

**Synthesis of {[Ru(bpy)<sub>2</sub>(2d)]<sub>3</sub>Ru}Cl<sub>8</sub> (GV5):** Complex **GV5** was synthesized in a manner identical to that described for **GV2**, except with **3d** (0.131 g, 1 mmol) in place of **3a**. Yield: 0.114 g, 84.1%; elemental analysis calcd (%) for C<sub>228</sub>H<sub>222</sub>Cl<sub>8</sub>N<sub>36</sub>O<sub>6</sub>Ru<sub>4</sub>: C 63.18, H 5.45, N 12.28; found: C 63.27, H 5.44, N 12.24; <sup>1</sup>H NMR (600 MHz, [D<sub>6</sub>]DMSO):  $\delta=9.24$  (d,  $J=30$  Hz, 12H), 8.89 (t,  $J=18$  Hz, 12H), 8.24–7.76 (m, 48H), 7.63 (t,  $J=9$  Hz, 12H), 7.37 (t,  $J=9$  Hz, 6H), 4.36 (t,  $J=15$  Hz, 12H), 1.90 (m, 12H), 1.45–0.50 ppm (m, 102H); MS (ESI, CH<sub>3</sub>OH):  $m/z$ : 545.8 ([ $M-8Cl-H$ ]<sup>7+</sup>), 635.9 ([ $M-8Cl-2H$ ]<sup>6+</sup>), 763.3 ([ $M-8Cl-3H$ ]<sup>5+</sup>), 953.6 ([ $M-8Cl-4H$ ]<sup>4+</sup>).

**Synthesis of {[Ru(bpy)<sub>2</sub>(2e)]<sub>3</sub>Ru}Cl<sub>8</sub> (GV6):** Complex **GV6** was synthesized in a manner identical to that described for **GV2**, except with **3e** (0.137 g, 1 mmol) in place of **3a**. Yield: 0.123 g, 87.2%; elemental analysis calcd (%) for C<sub>228</sub>H<sub>246</sub>Cl<sub>8</sub>N<sub>36</sub>O<sub>6</sub>Ru<sub>4</sub>: C 64.06, H 5.80, N 11.80; found: C 64.15, H 5.74, N 11.73; <sup>1</sup>H NMR (600 MHz, [D<sub>6</sub>]DMSO):  $\delta=9.23$  (d,  $J=30$  Hz, 12H), 8.88 (t,  $J=18$  Hz, 12H), 8.23–7.84 (m, 48H), 7.64 (t,  $J=12$  Hz, 12H), 7.37 (t,  $J=12$  Hz, 6H), 4.35 (s, 12H), 1.91 (m, 12H), 1.45–0.80 ppm (m, 126H); MS (ESI, CH<sub>3</sub>OH):  $m/z$ : 569.4 ([ $M-8Cl-H$ ]<sup>7+</sup>), 665.1 ([ $M-8Cl-2H$ ]<sup>6+</sup>), 797.8 ([ $M-8Cl-3H$ ]<sup>5+</sup>), 996.3 ([ $M-8Cl-4H$ ]<sup>4+</sup>).

## Determination of two-photon absorption cross-sections

The two-photon absorption spectra of the probes were determined over a broad spectral region by the typical two-photon-induced fluorescence (TPF) method relative to Rhodamine B in methanol as a standard.<sup>[20]</sup> Two-photon fluorescence data were acquired using an Opolette 355II spectrofluorimeter (pulse width  $\leq 100$  fs, 80 MHz repetition rate, tuning range 730–1010 nm, Spectra Physics Inc., USA). Two-photon fluorescence measurements were performed in fluorometric quartz cuvettes with **GV1–6** at  $2 \times 10^{-4}$  M in methanol. The experimental fluorescence excitation and detection conditions ensured negligible re-absorption processes, which can affect TPA measurements. The quadratic dependence of two-photon-induced fluorescence intensity on the excitation power was verified at an excitation wavelength of 830 nm. The two-photon absorption cross-section of the probes was calculated at each wavelength according to Equation (1).<sup>[14a]</sup>

$$\delta_2 = \delta_1 \frac{\phi_1 I_2 n_2}{\phi_2 C_2 I_1 n_1} \quad (1)$$

where  $I$  is the integrated fluorescence intensity,  $C$  is the concentration,  $n$  is the refractive index, and  $\phi$  is the quantum yield. Subscript “1” denotes the reference sample, and “2” denotes the samples under investigation.

## Preparation of DNA particles

DNA particles were prepared by incubating mixtures containing DNA and **GV1–6** at specific +/− ratios in 50 mM Tris-HCl (Tris = tris(hydroxymethyl)aminomethane) solution (pH 7.4) or in cell cul-

ture. These mixtures were then vortexed for 30 periods of various length to allow equilibration at room temperature.

### Gel retardation assay

Negatively supercoiled pBR322 DNA (7.5  $\mu\text{M}$ ) was treated with **GV1-6** in 50 mM Tris-HCl solution (pH 7.4), and the solutions were analyzed by electrophoresis for 1.5 h at 75 V on a 1% agarose gel in TBE buffer (89 mM Tris-borate acid, 2 mM EDTA, pH 8.3). The gel was stained with 1  $\mu\text{g mL}^{-1}$  ethidium bromide (EB) and photographed on an Alpha Innotech IS-5500 fluorescence, chemiluminescence, and visible imaging system.

### DNase-I protection assay

**GV1-6**-pBR322 DNA particles at a  $+/-$  ratio of 6.7 containing pBR322 DNA (1  $\mu\text{g}$ ) and free pBR322 DNA (1  $\mu\text{g}$ ) were incubated at 37  $^{\circ}\text{C}$  for 30 min in the presence of 1 unit of DNase-I in a digestion buffer consisting of 50 mM Tris-HCl (pH 7.4), 2.5 mM  $\text{MgCl}_2$ , and 0.5 mM  $\text{CaCl}_2$ . After DNase-I digestion, the solutions were treated with 5  $\mu\text{L}$  aliquots of 250 mM EDTA (pH 8.0) for 10 min to inactivate the DNase-I and then mixed with sodium dodecyl sulfate (SDS) in 0.1 M NaOH (pH 7.2) at a concentration of 1 wt%. Thereafter, the samples were incubated at room temperature for 2 h and then run electrophoretically for 1 h using 1% agarose gel in TBE buffer at 100 V.

### DNA binding assay

DNA binding experiments were performed at room temperature. UV/Vis spectra were recorded on a Perkin-Elmer Lambda 850 spectrophotometer and spectroscopic titrations were carried out in buffer A (5 mM Tris-HCl, 50 mM NaCl, pH 7.2). The DNA concentration per nucleotide was determined by absorption spectroscopy using the molar absorption coefficient ( $6600 \text{ M}^{-1} \text{ cm}^{-1}$ ) at 260 nm.<sup>[21]</sup> A solution of CT-DNA in the buffer gave a ratio of UV absorbances at 260 and 280 nm of 1.8–1.9:1, indicating that the DNA was sufficiently free of protein.<sup>[22]</sup>

Absorption titration experiments were performed by maintaining the **GV1-6** concentrations (4  $\mu\text{M}$ ) and varying the nucleotide concentration (0–40  $\mu\text{M}$ ) in buffer. The **GV1-6**-DNA solutions were incubated for 5 min prior to recording the absorption spectra. The intrinsic DNA binding constants  $K_b$  were determined according to Eq. (2):<sup>[23]</sup>

$$[\text{DNA}]/(\varepsilon_a - \varepsilon_f) = [\text{DNA}]/(\varepsilon_b - \varepsilon_f) + 1/K_b(\varepsilon_b - \varepsilon_f) \quad (2)$$

where [DNA] is the concentration of DNA in terms of base pairs, the apparent molar absorption coefficients  $\varepsilon_a$ ,  $\varepsilon_f$  and  $\varepsilon_b$  correspond to  $A_{\text{obsd}}/[\text{Ru}]$ , the molar extinction coefficient for the free ruthenium complex, and the molar extinction coefficient for the ruthenium complex in the fully bound form, respectively. A plot of  $[\text{DNA}]/(\varepsilon_a - \varepsilon_f)$  versus [DNA] gave a slope  $1/(\varepsilon_b - \varepsilon_f)$  and a y-intercept equal to  $1/K_b(\varepsilon_b - \varepsilon_f)$ . The intrinsic binding constant  $K_b$  is given by the ratio of the slope to the intercept.

### Dynamic light scattering and zeta potential assay

Dynamic laser light scattering equipment (Brookhaven BI-200SM) was used to determine the average hydrodynamic diameters and the zeta potentials of **GV1-6**-pBR322 DNA particles at various  $+/-$  ratios in 50 mM Tris-HCl solution (pH 7.4). Typically, six runs were performed for each solution and average values are reported.

### AFM imaging

The morphologies of the pBR322 DNA and **GV2-6**-pBR322 DNA particles at a  $+/-$  ratio of 6.7 were examined by AFM. A mica substrate was freshly cleaved by pulling off the top sheets with tape. After 1 min, a suspension of the substrate (10  $\mu\text{L}$ ) was applied by spin coating (1400 rpm, 30 s) and rinsed with distilled water (20  $\mu\text{L}$ ). AFM images were obtained in air at room temperature with an SPA400 atomic force microscope and an SPI3800N control station (Seiko Instruments) operated in tapping mode. Probes prepared from a single silicon crystal with a cantilever length of 129 nm and a spring constant of 33–62  $\text{N m}^{-1}$  (OMCLAC160TS-W2, Olympus) were used for imaging. Images were acquired in a 256  $\times$  256 pixels format and analyzed with the software provided with the imaging module.

### DNA photocleavage assay

Photo-induced DNA cleavage in the presence of **GV1-6** was examined by gel electrophoresis. Supercoiled pEGFP DNA (0.5  $\mu\text{g}$ ) was treated with **GV1-6** in 50 mM Tris-HCl solution (pH 7.4), and then the samples were irradiated at room temperature with an Xe lamp (450 nm, 150 W). After irradiation, the samples were mixed with sodium dodecyl sulfate (SDS) at a concentration of 1 wt%. Thereafter, the samples were incubated at room temperature for 2 h and then run electrophoretically for 1 h using 1% agarose gel in TBE buffer at 100 V.

### Continuous irradiation in the presence of CT-DNA

Continuous irradiation in the presence of CT-DNA was performed with a mercury vapor lamp (Osram HBO 200 W) and a 2000 W quartz halogen lamp (Philips), cooled by a water circulation system. IR (water) and UV ( $\text{KNO}_2$ ) cut-off filters were inserted between the irradiation cell and the excitation source. All of the experiments were performed with argon- and air-saturated solutions (2 mL) containing **GV1-6** (4  $\mu\text{M}$ ) and CT-DNA (40  $\mu\text{M}$ , bases).

### Cell line and cell culture

HeLa cells were obtained from the Cell Bank (Cell Institute, Sinica Academica Shanghai, Shanghai, China). All cell lines were maintained in DMEM medium supplemented with fetal bovine serum (10%), penicillin (100 units  $\text{mL}^{-1}$ ), and streptomycin (50 units  $\text{mL}^{-1}$ ) at 37  $^{\circ}\text{C}$  in a  $\text{CO}_2$  incubator (95% relative humidity, 5%  $\text{CO}_2$ ).

### Cell viability assay

The cytotoxicities of **GV1-6** and **GV1-6**-pEGFP DNA particles with and without 2 equivalents of DOPE at  $+/-$  ratios of 26.7 or 6.7 were evaluated in HeLa cells by MTT assay. At 3 days after seeding, the cells were counted by means of a hemocytometer and seeded into a 96-well cell-culture plate at a density of  $1 \times 10^4$  cells per well and then incubated for 24 h at 37  $^{\circ}\text{C}$  under 5%  $\text{CO}_2$ . The complexes were then added at the indicated concentrations to quadruplicate wells. After 48 h, stock MTT dye solution (20  $\mu\text{L}$ , 5  $\text{mg mL}^{-1}$ ) was added to each well and the microplates were incubated at 37  $^{\circ}\text{C}$  for 4 h. The medium was then removed, whereupon buffer (100  $\mu\text{L}$ ) containing DMSO (50%) and sodium dodecyl sulfate (20%) was added to the plates, which were shaken to dissolve the formazan products. A Tecan Infinite M200 monochromator-based multifunction microplate reader was used to measure the optical density of each well with background subtraction at 490 nm. The cell survival rate in the control wells without **GV1-6** solutions was considered as 100%.

### Cellular uptake of DNA particles

The cells were trypsinized, counted, and adjusted to  $1 \times 10^5$  cells mL<sup>-1</sup>, and 1 mL of medium was added per plate. After 24 h, the cell culture medium was replaced with serum-free DMEM (800  $\mu$ L). **GV1-6**-pEGFP DNA particles at +/– ratios of 26.7 or 6.7 containing pEGFP DNA (1  $\mu$ g) in serum-free DMEM (200  $\mu$ L) were added to the cells and the mixtures were incubated at 37 °C for 4 h.

For flow cytometric analysis, the cells were washed three times with PBS, trypsinized, and centrifuged in PBS. They were then harvested and a suspension of single cells in PBS (0.5 mL) was prepared and subjected to flow cytometric analysis. An FACSCanto II flow cytometer (BD Biosciences, USA) was used to measure the fluorescence intensity upon excitation at 488 nm.

For TEM imaging, cells were processed in situ, without removal from the culture dish. They were fixed in 0.1 M PBS containing 2.5% glutaraldehyde and 4% paraformaldehyde for 1 h. They were then rinsed with 0.1 M PBS, post-fixed in 1% osmium tetroxide solution (extremely toxic; use with caution) for 1 h, rinsed with distilled water, stained with 0.5% uranyl acetate for 1 h, dehydrated in a graded series of aqueous ethanol mixtures (30, 60, 70, 90, and 100% EtOH), and embedded in epoxy resin. The resin was polymerized at 60 °C for 48 h. Ultra-thin sections (50–75 nm) obtained with an LKB ultramicrotome were stained with 2% aqueous uranyl acetate and 2% aqueous lead citrate and imaged under a 120 kV FEI Tecnai Spirit TEM.

### One- and two-photon luminescent imaging

The cells were trypsinized, counted, and adjusted to  $1 \times 10^5$  cells mL<sup>-1</sup>, and 1 mL of the medium was placed in a laser confocal microscopy 35 mm<sup>2</sup> Petri dish (MatTek, USA). After 24 h, the cell culture medium was replaced with serum-free DMEM (800  $\mu$ L). **GV1-6**-pEGFP DNA particles at +/– ratios of 26.7 or 6.7 containing pEGFP DNA (1  $\mu$ g) in serum-free DMEM (200  $\mu$ L) were added to the cells and incubated at 37 °C for 4 h. The medium was then replaced with fresh DMEM containing 10% FBS, and the cells were incubated for a further 24 h.

After washing three times with fresh PBS (pH 7.0), the cells were imaged on a Zeiss LSM 710 NLO confocal microscope (63 $\times$ /NA 1.4 oil immersion objective). The excitation wavelength of the laser was 488 nm, and the emission spectra were integrated over the range 580–630 nm (single channel). For two-photon images, the excitation wavelength of the laser was 830 nm.

### Luciferase assay

HeLa cells were seeded into a 96-well cell-culture plate at a density of  $2 \times 10^4$  cells per well and then incubated for 24 h at 37 °C under 5% CO<sub>2</sub>. They were washed three times with PBS and the medium was replaced with serum-free DMEM. **GV1-6**-plasmid pGL3 control vector particles with or without 2 equivalents of DOPE at +/– ratios of 26.7 or 6.7 (corresponding to 0.2  $\mu$ g plasmid/well) were added to each well and the cells were incubated at 37 °C for 4 h. The medium was then replaced with fresh DMEM containing 10% FBS and the cells were incubated for a further 24 h. The gene activity was determined by comparing average fluorescence intensities of 10000 cells. Cells were washed with PBS, harvested, and treated for 30 min at 4 °C under end-over-end rotation with lysis buffer (50 mM Tris-HCl, pH 7.5, 150 mM NaCl, 2% Triton X-100, 2% NP40). The luciferase assay was carried out according to the manufacturer's protocol (Promega). Relative light units (RLU) were

measured with a Varioskan Flash (Thermo Scientific, USA) GloMax™ 96 microplate luminometer (Promega, USA).

### Acknowledgements

This work was supported by the 973 program (2014CB845604), the National Science Foundation of China (Nos. 21172273, 21171177, and 91122010), the Program for Changjiang Scholars and Innovative Research Teams in the University of China (No. IRT1298), and the Research Fund for the Doctoral Program of Higher Education (20110171110013).

**Keywords:** DNA · fluorescent probes · non-viral gene delivery · ruthenium(II) complexes · two-photon luminescence

- [1] a) D. Luo, W. M. Saltzman, *Nature Biotech.* **2000**, *18*, 32–36; b) C. E. Thomas, A. Ehrhardt, M. A. Kay, *Nat. Rev. Genet.* **2003**, *4*, 346–358; c) T. Niidome, L. Huang, *Gene Ther.* **2002**, *9*, 1647–1652; d) C. X. He, Y. Tabata, J. Q. Gao, *Inter. J. Pharm.* **2010**, *386*, 232–242; e) O. M. Merkel, T. Kissel, *Acc. Chem. Res.* **2012**, *45*, 961–970.
- [2] C. Y. M. Hsu, U. Hasan, *J. Drug Targeting* **2012**, *20*, 301–328.
- [3] a) W. T. Godbey, K. K. Wu, A. G. Mikos, *Proc. Natl. Acad. Sci. USA* **1999**, *96*, 5177–5181; b) R. Savic, L. Luo, A. Eisenberg, D. Maysinger, *Science* **2003**, *300*, 615–618; c) N. D. Sonawane, F. C. Szoka, A. S. Verkman, *J. Biol. Chem.* **2003**, *278*, 44826–44831; d) I. Roy, T. Y. Ohulchanskyy, D. J. Bharali, H. E. Pudavar, R. A. Mistretta, N. Kaur, P. N. Prasad, *Proc. Natl. Acad. Sci. USA* **2005**, *102*, 279–284.
- [4] a) B. N. G. Giepmans, S. R. Adams, M. H. Ellisman, R. Y. Tsien, *Science* **2006**, *312*, 217–224; b) B. Dubertret, P. Skourides, D. J. Norris, V. Noireaux, A. H. Brivanlou, A. Libchaber, *Science* **2002**, *298*, 1759–1762; c) G. P. Pfeifer, Y. H. You, A. Besaratinia, *Mutat. Res.* **2005**, *571*, 19–31.
- [5] W. R. Zipfel, R. M. Williams, W. W. Webb, *Nat. Biotechnol.* **2003**, *21*, 1369–1377.
- [6] U. Resch-Genger, M. Grabolle, S. Cavaliere-Jaricot, R. Nitschke, T. Nann, *Nat. Methods* **2008**, *5*, 763–775.
- [7] U. K. Tirlapur, K. Konig, *Nature* **2002**, *418*, 290–291.
- [8] a) K. E. Erkkila, D. T. Odom, J. K. Barton, *Chem. Rev.* **1999**, *99*, 2777–2796; b) Q. Zhao, F. Li, C. Huang, *Chem. Soc. Rev.* **2010**, *39*, 3007–3030; c) K. H. Leung, H. Z. He, V. P. Y. Ma, H. J. Zhong, D. S. H. Chan, J. Zhou, J. L. Mergny, C. H. Leung, D.-L. Ma, *Chem. Commun.* **2013**, *49*, 5630–5632; d) H. Z. He, K. H. Leung, W. Wang, D. S. H. Chan, C. H. Leung, D. L. Ma, *Chem. Commun.* **2014**, *50*, 5313–5315; e) D. L. Ma, S. Lin, K. H. Leung, H. J. Zhong, L. J. Liu, D. S. H. Chan, A. Bourdoncle, J. L. Mergny, H. M. D. Wang, C. H. Leung, *Nanoscale* **2014**, *6*, 8489–8494.
- [9] E. Bagdaley, M. R. Gill, N. H. Green, D. Turton, I. V. Sazanovich, S. W. Botchway, C. Smythe, J. W. Haycock, J. A. Weinstein, J. A. Thomas, *Angew. Chem. Int. Ed.* **2014**, *53*, 3367–3371; *Angew. Chem.* **2014**, *126*, 3435–3439.
- [10] W. Xu, J. Zuo, L. Wang, L. Ji, H. Chao, *Chem. Commun.* **2014**, *50*, 2123–2125.
- [11] P. Zhang, L. Pei, Y. Chen, W. Xu, Q. Lin, J. Wang, J. Wu, Y. Shen, L. Ji, H. Chao, *Chem. Eur. J.* **2013**, *19*, 15494–15503.
- [12] a) L. Liu, H. Zhang, X. Meng, J. Yin, D. Li, C. Liu, *Biomaterials* **2010**, *31*, 1380–1391; b) J. Yin, X. Meng, S. Zhang, D. Zhang, L. Wang, C. Liu, *Biomaterials* **2012**, *33*, 7884–7894; c) X. Dong, X. Wang, Y. He, Z. Yu, M. Lin, C. Zhang, J. Wang, Y. Song, Y. Zhang, Z. Liu, Y. Li, Z. Guo, *Chem. Eur. J.* **2010**, *16*, 14181–14189; d) B. L. Yu, Y. Chen, C. Ouyang, H. Y. Huang, L. N. Ji, H. Chao, *Chem. Commun.* **2013**, *49*, 810–812; e) T. Kikuchi, S. Sato, D. Fujita, M. Fujita, *Chem. Sci.* **2014**, *5*, 3257–3260; f) J. Malina, N. P. Farrell, V. Brabec, *Inorg. Chem.* **2014**, *53*, 1662–1671.
- [13] B. Wang, M. R. Wasielewski, *J. Am. Chem. Soc.* **1997**, *119*, 12–21.
- [14] a) C. Xu, W. W. Webb, *J. Opt. Soc. Am. B* **1996**, *13*, 481–491; b) N. S. Markarov, M. Drobnizhev, A. Rebane, *Optics Express* **2008**, *16*, 4029–4047.
- [15] S. A. Ezadyar, A. S. Kumbhar, A. A. Kumbhar, A. Khan, *Polyhedron* **2012**, *36*, 45–55.

- [16] M. Eriksson, M. Mehmedovic, G. Westman, B. Akerman, *Electrophoresis* **2005**, *26*, 524–532.
- [17] C. C. Ju, A. G. Zhang, C. L. Yuan, X. L. Zhao, K. Z. Wang, *J. Inorg. Biochem.* **2011**, *105*, 435–443.
- [18] a) J. Yang, K. Takeyasu, Z. F. Shao, *FEBS Lett.* **1992**, *301*, 173–176; b) Y. Liu, Z. L. Yu, Y. M. Zhang, D. S. Guo, Y. P. Liu, *J. Am. Chem. Soc.* **2008**, *130*, 10431–10439.
- [19] F. Sansone, M. Dudić, G. Donofrio, C. Rivetti, L. Baldini, A. Casnati, S. Cellai, R. Ungaro, *J. Am. Chem. Soc.* **2006**, *128*, 14528–14536.
- [20] G. A. Crosby, J. N. Demas, *J. Phys. Chem.* **1971**, *75*, 991–1024.
- [21] J. Marmur, *J. Mol. Biol.* **1961**, *3*, 208–218.
- [22] M. E. Reichmann, S. A. Rice, C. A. Thomas, P. Doty, *J. Am. Chem. Soc.* **1954**, *76*, 3047–3053.
- [23] A. Wolfe, G. H. Shimer Jr., T. Meehan, *Biochemistry* **1987**, *26*, 6392–6397.

---

Received: September 5, 2014

Published online on January 16, 2015